RECENT DEVELOPMENTS IN METHODS FOR CALCULATING TRANSONIC FLOWS OVER WINGS

M. G. Hall and M. C. P. Firmin
Royal Aircraft Establishment
Farnborough, Hampshire, England

Abstract

The paper is in two main parts. In the first, recent progress is described in the development of a finite-difference method for inviscid three-dimensional flows about arbitrary wings, based on a new transonic small-perturbation approximation, the rotated or split difference scheme of Albone and Jameson and the relaxation technique of Murman and Cole. An account is given of the formulation of the problem, the transformation to a new coordinate system, and the numerical method of solution. Comparisons are given with solutions by other methods and with experimental measurements for an example in which viscous effects are expected to be relatively small.

The second part of the paper is concerned with the estimation of viscous effects in flows about two-dimensional aerofoils. A method is evolved which requires modification to the boundary conditions at the aerofoil surface and along the dividing streamline, in methods normally used for inviscid flow. In the calculation, methods for the calculation of the viscous layers, which are assumed to be turbulent except near the nose of the aerofoil, are combined iteratively with the modified inviscid flow method. Comparisons with experiments include cases where the calculation of the inviscid flow is itself iterative and weak shock waves are present.

I. Preliminary remarks

There are several reasons for attempting to improve aerodynamic design. Aircraft manoeuvrability or operating economy can be improved, for example. It has been estimated(1) that the exploitation, in transport aircraft design, of recent advances in transonic aerodynamics should enable a doubling of aviation fuel costs, relative to other costs, to be compensated for entirely. Our aim here has been to improve the aerodynamic design of aircraft in the transonic régime by providing the designer with advanced calculation methods. The work has now reached a stage where transonic flows about arbitrary wings can be calculated to a reasonable approximation and the methods are actually used in practical design. However, much more remains to be done. In particular, the accuracy of the inviscid methods needs to be improved, and the treatment of viscous effects, of shock waves and their interactions with boundary layers, of combined wing-body configurations and of the inverse design problem all require attention.

Our work is part of the growing stream started by Murman and Cole.(2) Their introduction of a relaxation technique for calculating mixed subsonic-supersonic flows has transformed an almost totally barren scene into one of the fruitful abundance. With the aid of the ideas of Albone(3) and Jameson(4) who independently showed, with their equivalent 'split' or 'rotated' difference schemes, how coordinate systems could be chosen to suit the body geometry or for other reasons rather than be limited by the geometry of the flow, a wide variety of problems can now be treated.

In the first part of this paper a method developed by Albone, Hall and Joyce(5) for calculating the inviscid three-dimensional flow about arbitrary wings is described. The method is based on a transonic small-perturbation approximation rather than the exact equations, on the following argument. For practical purposes, we wish to be able to treat wings with arbitrary planforms and arbitrary spanwise variations of section and twist. To satisfy exactly the flow-tangency boundary condition on the surface of such a wing would be a very formidable task even if the problem proved in present circumstances tractable. Thus, the solution of the exact equations would, at least, be a lengthy process. On the other hand, experience(6) with two-dimensional problems has shown that the transonic small-perturbation equation for the velocity potential can yield results that are for practical purposes satisfactorily close to solutions of the exact equation, even when the free-stream Mach number is not near 1 and the perturbations are far from small. (See, for example, Figs.16 and 17.) Because the flow-tangency boundary conditions are in such a case satisfied on a plane and not on the actual surface, a transonic small-perturbation problem can be formulated for arbitrary wings without the difficulty associated with an exact treatment of the boundary conditions. Moreover, such a formulation enables the inverse design problem and viscous effects, which are also of practical importance, to be treated readily.

In the second part a scheme is outlined by which an allowance is made for the boundary layer and wake when determining the pressure distribution on aerofoils. Although the method has so far been limited to attached flow, it turns out that even for this case very important changes in pressure distribution can occur for aerofoils having significant rear loading or when there are shock waves. This suggests that an allowance for the viscous layer should be included in design methods for three-dimensional wings.

II. Inviscid transonic flows over wings

Introduction

The method developed by Albone, Hall and Joyce(5) is similar in some respects to the revised version of the method of Ballhaus and Bailey(7) described by Bailey(8) in his recent survey of the computation of transonic flows by relaxation methods. For each method the successive line relaxation technique of Murman and Cole is adopted, in which the key is the use of different finite-difference approximations for the subsonic and supersonic parts of the flow. And for each method the split or rotated difference schemes of Albone(3) and Jameson(4) are employed to enable an efficient wing-oriented coordinate system to be adopted. The essential point here is that, to avoid the numerical instability that arises when the domain of dependence for the difference equation does not include that for the differential equation, one can split

the derivatives in the differential equation into components according to the canonical or flow-oriented form of the equation and approximate these components by finite differences according to how one would approximate the related derivatives in the canonical form.

However, in other respects there are significant differences between the two methods. The transonic small-perturbation equation that we solve differs from that solved by Bailey in having extra terms. Bailey's form of equation is the commonly used equation derived by Cole[9] and, in Cole's approximation, strictly valid only for wings of very high aspect ratio. Our form of equation arises from a new formulation of the transonic small-perturbation problem for arbitrary wing planforms. While Bailey uses a non-uniform mesh to achieve the variations in mesh density required for both accuracy and economy, we employ coordinate stretchings which meet the same requirement but permit the use of a uniform mesh in the computing space. Moreover, these coordinate stretchings are used to transform the infinite physical space into a finite computing space and thus avoid Bailey's need to use an approximate analytical expression for the far field. There are, in addition, minor differences in the treatment of the flow tangency boundary conditions and the Kutta condition.

The present account begins with the formulation of the transonic small-perturbation problem for arbitrary wings. This includes a rearrangement of the exact equation for the velocity potential so that the derivatives are appropriately split, the derivation of the transonic small-perturbation equation, and statements of the boundary and Kutta conditions. Next, the various transformations made for convenience, accuracy and economy are outlined and applied. Then the numerical method of solution, involving the setting-up and solution of finite-difference equations, is briefly described. Some numerical results are presented, including comparisons with other solutions and with experimental measurements. Finally, an assessment of the method is given, with a note of its shortcomings and of the developments that might be expected in the future.

Formulation of the transonic small-perturbation problem

Exact equation. The desired form of the exact equation for the velocity potential Φ, in rectangular cartesian coordinates x, y, z, is obtained from the canonical form of the governing equation, written in terms of coordinates x' in the local stream direction and y' and z' normal to the stream,

$$\underline{(a^2 - q^2)\Phi_{x'x'}} + a^2\Phi_{y'y'} + a^2\Phi_{z'z'} = 0 \quad , \qquad (1)$$

where a and q are the local values of the speed of sound and of the stream speed respectively, related by

$$a^2 = \frac{\gamma - 1}{2} + \frac{1}{M_\infty^2} - \frac{\gamma - 1}{2} q^2 \quad , \qquad (2)$$

where M_∞ is the free-stream Mach number and the free-stream velocity has been taken to be of unit magnitude.

The underlined term in equation (1) is that which, following Murman and Cole, would for numerical stability be approximated by a backward difference when the local flow is supersonic. The other terms would always be approximated by central differences, while the underlined term would be approximated by a central difference only when the flow is locally subsonic.

A transformation from the x', y', z' system to the x, y, z system is now made by rotating the coordinate axes. If the terms arising from the above underlined term are themselves underlined and kept separate from the others, equation (1) becomes

$$\frac{1}{q^2}(a^2 - q^2)\left[\underline{u^2\Phi_{xx} + v^2\Phi_{yy} + w^2\Phi_{zz} + 2uv\Phi_{xy} + 2uw\Phi_{xz} + 2vw\Phi_{yz}}\right]$$
$$+ \frac{a^2}{q^2}\left[(q^2 - u^2)\Phi_{xx} + (q^2 - v^2)\Phi_{yy} + (q^2 - w^2)\Phi_{zz} - 2uv\Phi_{xy} - 2uw\Phi_{xz} - 2vw\Phi_{yz}\right] = 0 \qquad (3)$$

where u, v and w are the velocity components, given by $u = \Phi_x$, $v = \Phi_y$ and $w = \Phi_z$, and $q^2 = u^2 + v^2 + w^2$.

This equation is no more than a rearrangement of the standard equation for the velocity potential, in which each of the second derivatives has been split into two parts. The Albone-Jameson procedure is to approximate only the underlined term by backward differences when the flow is locally supersonic. Otherwise central-difference approximations are used.

Transonic small-perturbation approximation. The transonic small-perturbation equation may be derived from the exact equation (3) in a number of ways and we give here a derivation in which the scaling of variables is avoided but the physical meaning of the basic assumptions is stressed.

Firstly, the velocity potential Φ is replaced by a perturbation potential ϕ defined by

$$\Phi \equiv x + \phi \quad , \qquad (4)$$

where the free-stream velocity is taken to be in the x-direction. The velocity components are now

$$\left.\begin{aligned} u &= 1 + \phi_x \\ v &= \phi_y \\ w &= \phi_z \end{aligned}\right\} \quad . \qquad (5)$$

The small-perturbation assumption consists in assuming that the perturbation in velocity is small. Thus ϕ_x, ϕ_y and ϕ_z must all be small. If, as shown in Fig.1, the z-axis is taken in the vertical direction the slope $\partial z/\partial x$ of the wing surface relative to the horizontal plane z = const. is given by w/u approximately, except possibly for shapes of very low aspect ratio, which we exclude. It follows that the slope w/u must also be small. It is convenient to write

$$\frac{w}{u} \sim \delta \quad , \quad \delta \ll 1 \quad . \qquad (6)$$

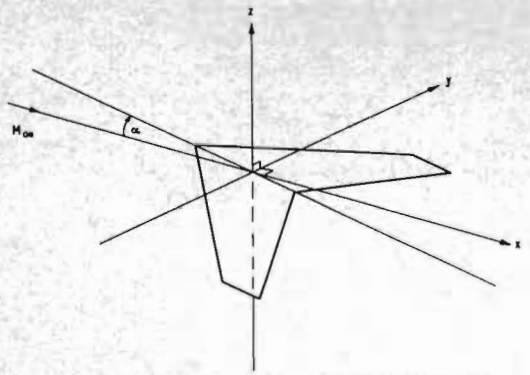

Fig.1 Coordinate system in physical space

The small-perturbation approximation cannot therefore be strictly valid in the neighbourhood of a blunt leading edge but, as for aerofoils, we accept this inconsistency and proceed. It is also convenient to take a typical streamwise chord of the wing to be of unit length, so the condition $\phi_x \ll 1$ implies that $\phi \ll 1$ and we write

$$\phi \sim \varepsilon , \quad \varepsilon \ll 1 . \tag{7}$$

Now we introduce two lengths $\underline{b}$ and $\underline{c}$ in the y and z directions respectively, such that

$$\left.\begin{aligned} \phi_y &\sim \varepsilon/\underline{b} \\ \phi_z &\sim \varepsilon/\underline{c} \end{aligned}\right\} . \tag{8}$$

The length $\underline{b}$ is related to the planform of the wing. Thus for any wing of aspect ratio ~ 1, or of any aspect ratio but appreciable (though not very high) sweep, $\underline{b} \sim 1$. On the other hand, for a wing of high aspect ratio and small sweep, $\underline{b} \gg 1$. This is consistent with the exact relation $\phi_y = -\phi_x \tan \Lambda$ for an infinite cylindrical wing swept at an angle Λ. The length $\underline{c}$ is related to the wing slope $w/u \sim \delta$, since $\phi_z = w/u$ approximately, so that

$$\varepsilon/\underline{c} \sim \delta . \tag{9}$$

Other relations to wing geometry will emerge.

The next step is to expand the terms in equation (3) in the new dependent variable ϕ, by making use of the conditions

$$\left.\begin{aligned} \phi &\sim \varepsilon \ll 1 \\ \phi_y &\sim \varepsilon/\underline{b} \ll 1 \\ \phi_z &\sim \varepsilon/\underline{c} \ll 1 \end{aligned}\right\} . \tag{10}$$

Thus, on omitting quantities of third and higher order, and on substituting in equation (3), we have

$$\underline{\left[1 - M_\infty^2 - (\gamma+1)M_\infty^2\phi_x\right]\phi_{xx}} + 2\underline{\left(1 - M_\infty^2\right)\left[\phi_y\phi_{xy} + \phi_z\phi_{xz}\right]} + \left[1 - (\gamma-1)M_\infty^2\phi_x\right](\phi_{yy} + \phi_{zz}) - 2\phi_y\phi_{xy} - 2\phi_z\phi_{xz} = 0 . \tag{11}$$

To the first-order, the pressure coefficient is given by

$$C_p = -2\phi_x . \tag{12}$$

The small-perturbation equation (11) is now further simplified by making a transonic flow approximation. We suppose that $1 - M_\infty^2 \sim \phi_x$, that is

$$1 - M_\infty^2 \sim \varepsilon . \tag{13}$$

Thus the second of the underlined terms in equation (11) can be omitted. Furthermore, according to the equation, $(\phi_{yy} + \phi_{zz}) \sim \phi_x\phi_{xx} (\sim \varepsilon^2)$, $\phi_y\phi_{xy} (\sim \varepsilon^2/\underline{b}^2)$ or $\phi_z\phi_{xz} (\sim \varepsilon^2/\underline{c}^2)$ whichever is the largest, even though $\phi_{yy} \sim \varepsilon/\underline{b}^2$ and $\phi_{zz} \sim \varepsilon/\underline{c}^2$. Hence the term $(\gamma - 1)M_\infty^2\phi_x(\phi_{yy} + \phi_{zz})$ can be omitted. The result is the transonic small-perturbation equation for arbitrary wings

$$\underline{\left[1 - M_\infty^2 - (\gamma+1)M_\infty^2\phi_x\right]\phi_{xx}} + \phi_{yy} + \phi_{zz} - 2\phi_y\phi_{xy} - 2\phi_z\phi_{xz} = 0 \tag{14}$$

where backward differences are to be used for the underlined term when the local flow is supersonic. This equation differs from the commonly adopted equation (see Bailey[8]) in having additional terms $2\phi_y\phi_{xy}$ and $2\phi_z\phi_{xz}$.

Note that for $\underline{b} \sim 1$, that is, for wings of aspect ratio ~ 1, or for wings of any aspect ratio but appreciable (though not very high) sweep, $(\phi_{yy} + \phi_{zz}) \ll \varepsilon$. Yet $\phi_{yy} \sim \varepsilon$, so it follows that $\phi_{zz} \sim \varepsilon$ and the length $\underline{c} \sim 1$. However, for $b \to \infty$, that is, for a flow approaching that past a two-dimensional aerofoil, $\phi_{yy} \to 0$ and $\phi_y\phi_{xy} \to 0$, while $\phi_z\phi_{xz} (\sim \varepsilon^2/\underline{c}^2) \ll \phi_{zz} (\sim \varepsilon/\underline{c}^2)$, and the equation reduces to the well-known form

$$\underline{\left[1 - M_\infty^2 - (\gamma+1)M_\infty^2\phi_x\right]\phi_{xx}} + \phi_{zz} = 0 , \tag{15}$$

which implies that $\phi_{zz} \sim \varepsilon^2$ so that $\underline{c} \sim \varepsilon^{-\frac{1}{2}}$, that is $\underline{c} \gg 1$. From the relations (7) and (9) it follows that the perturbation potential $\phi \sim \underline{c}\delta$ and is larger for a two-dimensional aerofoil than for a three-dimensional wing of the same thickness. A summary of some of the differences between wings and aerofoils is shown in the table below.

Quantity	Wing	Aerofoil
$\underline{b}$, length scale in transverse y-direction	1	∞
$\underline{c}$, length scale in vertical z-direction	1	$\delta^{-1/3}$
ϕ, perturbation potential	δ	$\delta^{2/3}$
$1 - M_\infty^2$	δ	$\delta^{2/3}$
ϕ_x, ~ pressure coefficient	δ	$\delta^{2/3}$
ϕ_{xx}, ~ streamwise pressure gradient	δ	$\delta^{2/3}$
ϕ_{xz}, ~ vertical pressure gradient	δ	δ
$\phi_x\phi_{xx}$	δ^2	$\delta^{4/3}$
$(\phi_{yy} + \phi_{zz})$ terms in governing differential equation	δ^2	$\delta^{4/3}$
$\phi_z\phi_{xz}$	δ^2	δ^2

TABLE 1 MAGNITUDE OF VARIOUS QUANTITIES, FOR WINGS AND AEROFOILS

Certain comments on the above may be made. For the aerofoil, the magnitudes that have emerged for $\underline{c}$, ϕ and $1 - M_\infty^2$ show that if new scaled quantities of unit order of magnitude are to be defined then the appropriate scaling is obtained by putting

$$\left.\begin{aligned} \bar{z} &\sim \delta^{1/3} z \\ \bar{\phi} &\sim \delta^{-2/3} \phi \\ K &\sim \frac{1 - M_\infty^2}{\delta^{2/3}} \end{aligned}\right\} . \qquad (16)$$

These will be recognised as the scaled quantities actually used by Cole,[9] Murman and Cole[2] and others. Equation (15) can thus be reduced to the familiar similarity form

$$\left[K - (\gamma + 1)\bar{\phi}_{\bar{x}}\right]\bar{\phi}_{\bar{x}\bar{x}} + \bar{\phi}_{\bar{z}\bar{z}} = 0 \quad . \qquad (17)$$

This is used in the calculations described in the second part of the present paper. For a wing the corresponding scaled quantities are different. They are

$$\left.\begin{aligned} \bar{z} &\sim z \\ \bar{\phi} &\sim \delta^{-1} \phi \\ K &\sim \frac{1 - M_\infty^2}{\delta} \end{aligned}\right\} . \qquad (18)$$

The difference between the relations (16) and (18) does not seem to have been recognised. For example, Bailey[8] uses the same scaling (16) for wings as for aerofoils. Note, moreover, that from inspection of equation (14) it does not seem possible to define similarity parameters like K such that the solution depends only on K (as with aerofoils) and not on the thickness δ as well. In other words, there does not appear to be a simple transonic similarity rule for wings as there is for aerofoils.

The differences in the vertical length scale c and the perturbation potential ϕ imply differences in the physical flow fields. The pressures, and streamwise pressure gradients, on the wing surface are smaller by a factor $\sim\delta^{1/3}$ than those on the corresponding aerofoil surface. For a wing the normal and streamwise pressure gradients are of the same order of magnitude, but for an aerofoil the normal gradients are smaller than the streamwise gradients by a factor $\sim\delta^{1/3}$.

The final comment on the differences between wings and aerofoils relates to the terms retained in the governing differential equation, in the transonic small-perturbation approximation. If $(\phi_{yy} + \phi_{zz})$ is considered as a single term all the terms in equation (14) are the same order of magnitude, δ^2 , when $\bar{b} \sim 1$ and the equation is applied to the flow past wings. In particular $\phi_z\phi_{xz}$ and $\phi_y\phi_{xy}$ are the same order of magnitude as $\phi_x\phi_{xx}$. However, when $\bar{b} \to \infty$ and the equation is applied to the flow past aerofoils, $\phi_z\phi_{xz}$ is smaller than other terms like $\phi_x\phi_{xx}$ by a factor $\sim\delta^{2/3}$.

Just as for aerofoils, we wish to extend the use of the transonic small-perturbation equation (14) to the calculation of flows with speeds that are not near-sonic and with perturbations that are not small. In these circumstances rigid adherence to the precise form of the equation is unjustified and modifications are acceptable for expedience or accuracy. To admit some flexibility, therefore, we replace the equation by

$$\left[1 - M_\infty^p - (\gamma + 1)M_\infty^p\phi_x\right]\phi_{xx} + \phi_{yy} + \phi_{zz} - 2q\phi_y\phi_{zy} - 2r\phi_z\phi_{xz} = 0 \quad , \qquad (19)$$

where p is a constant and q and r are each either unity or zero depending on whether we wish to retain or omit the terms $2\phi_y\phi_{xy}$ and $2\phi_z\phi_{xz}$ respectively. The introduction of the exponent p is of course within the bounds of the transonic approximation, because $M_\infty^p = M_\infty^2[1 + 0(\delta)]$. The term $2\phi_z\phi_{xz}$ would be expected to create numerical difficulties when leading edges are very blunt and the simplest expedient then would be to set $r = 0$. When $p = 2$ and $q = r = 0$ the equation reduces to the commonly accepted equation of Cole,[9] Ballhaus and Bailey[7] and others.

Boundary conditions. The flow-tangency boundary conditions takes the familiar linearized form

$$(\phi_z)_{z=0} = \left(\frac{\partial z_s}{\partial x}\right)_{\alpha=0} - \alpha \quad , \qquad (20)$$

where α is the angle of incidence of the wing relative to the free stream and the wing surface is given by $z = z_s(x,y)$ when $\alpha = 0$. Note that this boundary condition is satisfied on the plane $z = 0$ through the wing and not on the wing surface.

The boundary conditions at an infinite distance from a finite wing differ greatly from those in two dimensions. Except for the downstream direction the perturbation potential tends to zero everywhere with increasing distance from the wing. Thus, with the coordinate axes shown in Fig.1, we have for

$$\left.\begin{aligned} x \to -\infty \quad , \quad y \to \pm\infty \quad \text{or} \quad z \to \pm\infty \quad , \\ \phi \to 0 \quad . \end{aligned}\right\} . \qquad (21)$$

Far downstream at $x = +\infty$ the perturbation potential ϕ satisfies the reduced equation

$$\phi_{yy} + \phi_{zz} = 0 \qquad (22)$$

subject to the conditions

$$\left.\begin{aligned} \phi(z=+0) - \phi(z=-0) &= \begin{cases} \Gamma(y) \\ 0 \end{cases} \text{for } y \gtrless y \text{ (semi-span)} \\ \phi(z \to \pm\infty) &\to 0 \quad , \end{aligned}\right\} \qquad (23)$$

where $\Gamma(y)$ is equal to the difference in ϕ across the trailing edge of the wing at the station y and is a measure of the strength of the trailing vortex sheet.

For wings that are symmetrical about the vertical section $y = 0$ we have the symmetry conditions

$$y = 0 \quad , \quad \phi_y = \phi_{xy} = 0 \quad . \qquad (24)$$

The numerical method described here is concerned with this case.

Kutta condition. The pressure and flow direction are required to be continuous across the trailing vortex sheet. In the small-perturbation approximation it suffices if ϕ_x and ϕ_z are continuous across $z = 0$. It follows that the jump in ϕ across the vortex sheet is independent of x , for $y = \text{const}$. Thus the conditions to be satisfied can be written

$$\left.\begin{aligned} [\phi(z = +0) - \phi(z = -0)]_{x>x_{te}} &= \Gamma(y) \\ \text{where} \qquad \Gamma(y) &\equiv [\phi(z = +0) - \phi(z = -0)]_{x=x_{te}} \\ \phi_z(z = +0) &= \phi_z(z = -0) \ , \end{aligned}\right\} \quad (25)$$

and $x = x_{te}$ at the trailing edge.

Coordinate transformation

Transformation to near-rectangular planform. We first make an intermediate transformation which has as its main purpose the alignment of coordinate lines with the leading and trailing edges of the wing, so that the mesh density needed for accuracy can be obtained economically. Accordingly, we replace the variable x by $x^*(x,y)$ where

$$x^* = \frac{x - g_1(y)}{g_2(y) - g_1(y)} - \text{const.} \quad . \qquad (26)$$

As shown in Fig.2 the functions $g_1(y)$ and $g_2(y)$ define curves which follow the leading and trailing edges respectively, except at the centre section $y = 0$ and at the wing tip. In the x^*, y plane the planform is nearly rectangular, with sweep, taper and cranking all removed. The functions $g_1(y)$ and $g_2(y)$ are chosen to depart smoothly from the wing planform and are continued analytically. At the centre-section they intersect the x axis at right angles, to simplify the application of the symmetry condition. Beyond the wing tip they tend asymptotically to a pair of lines parallel to the y axis.

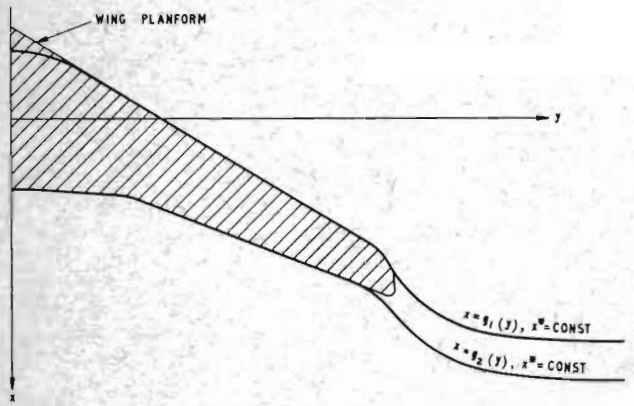

Fig.2 Wing-oriented coordinate lines $x^* = \text{const.}$ in physical space

Coordinate stretching. We complete the coordinate transformations by introducing separate stretchings of the x^*, y and z ordinates, to transform the infinite physical space to a finite computing space and to provide increases of mesh density in the physical space where they are needed. Accordingly, we replace x^*, y and z by $X(x^*)$, $Y(y)$ and $Z(z)$ respectively where

$$\left.\begin{aligned} X &= (1 - a_1)X_1(x^*) + a_1X_2(x^*) \\ Y &= (1 - b_1)Y_1(y) + b_1[b_2Y_2(y) + b_3Y_3(y)] \\ Z &= Z_1(z) \end{aligned}\right\} \quad (27)$$

where a_1, b_1, b_2 and b_3 are constant. The functions $X_1(x^*)$, $X_2(x^*)$, $Y_1(y)$, $Y_2(y)$, $Y_3(y)$ and $Z_1(z)$ are all simple analytic functions. Essentially X_1, Y_1 and Z_1 provide a fairly uniform mesh density near the wing and a gradual reduction of density with increasing distance from the wing, and are such that

$$\left.\begin{aligned} X(x^* = \pm\infty) &= \pm 1 \\ Y(y = \infty) &= 1 \\ Z(z = \pm\infty) &= \pm 1 \end{aligned}\right\} \quad . \qquad (28)$$

The functions X_2, Y_2 and Y_3 respectively provide higher mesh densities near the leading edge, the centre-section and the wing tip.

The problem in the transformed coordinates. Replacement of the dependent variables x, y, z in the governing equation (19) by the new stretched variables X, Y, Z defined in equations (26) and (27) yields

$$\underline{A^*\phi_{XX}} + A\phi_{XX} + B\phi_{YY} + C\phi_{ZZ} + 2D\phi_{XY} + 2E\phi_{XZ} + \underline{G^*} + G = 0 \qquad (29)$$

where

$$\underline{A^*} = \left[1 - M_\infty^p - (\gamma + 1)M_\infty^p X_x \phi_{\underline{X}}\right] X_x^2$$

$$A = X_y\left[X_y - 2qX_x(X_y\phi_X + Y_y\phi_y)\right]$$

$$B = Y_y^2$$

$$C = Z_z^2$$

$$D = Y_y\left[X_y - qX_x(X_y\phi_X + Y_y\phi_Y)\right]$$

$$E = -rX_xZ_z^2\phi_Z$$

$$\underline{G^*} = \left[1 - M_\infty^p - (\gamma + 1)M_\infty^p X_x \phi_{\underline{X}}\right] X_{xx}\phi_X$$

$$G = Y_{yy}\phi_Y + Z_{zz}\phi_Z + \left[X_{yy} - 2qX_{xy}(X_y\phi_X + Y_y\phi_Y)\right]\phi_X \ .$$

Note that the derivatives ϕ_{XX} and ϕ_X in the computing system X, Y, Z are split into an underlined part to be approximated by backward differences and a part to be approximated by central differences, for supersonic flow. All other terms are to be approximated by central differences whether the flow is subsonic or supersonic. We consider the flow to be subsonic when $\underline{A}^* > 0$ and supersonic when $\underline{A}^* < 0$, which is strictly correct to first-order only.

The flow-tangency boundary condition (20) becomes

$$\phi_Z(Z = 0) = \frac{1}{Z_z}\left[\left(\frac{\partial z_s}{\partial x}\right)_{\alpha=0} - \alpha\right] \quad . \qquad (30)$$

The far-field boundary conditions (21), (22) and (23) become

$$\left.\begin{aligned} &\text{for} \quad X = -1 \ , \quad Y = 1 \quad \text{or} \quad Z = \pm 1 \\ &\qquad\qquad \phi = 0 \ ; \end{aligned}\right\} \quad (31)$$

$$\text{for} \quad X = +1 \ ,$$

$$Y_y^2\phi_{YY} + Y_{yy}\phi_Y + Z_z^2\phi_{ZZ} + Z_{zz}\phi_Z = 0 \ , \qquad (32)$$

subject to

$$\left.\begin{aligned} \phi(Z=+0) - \phi(Z=-0) &= \begin{cases} \Gamma(Y) \\ 0 \end{cases} \text{for } Y \gtrless Y \text{ (semi-span)} \\ \phi(Z = \pm 0) &= 0 \ . \end{aligned}\right\} \quad (33)$$

The symmetry condition (24) reduces to

$$Y = 0 \quad , \quad \phi_Y = \phi_{XY} = 0 \quad , \qquad (34)$$

because the lines $g_1(y)$ and $g_2(y)$ intersect the plane of symmetry $Y = 0$ at right angles, so that $X_y = 0$ there.

Finally, the Kutta condition (25) becomes

$$\left.\begin{aligned} &\left[\phi(Z = +0) - \phi(Z = -0)\right]_{X>X_{te}} = \Gamma(Y) \\ \text{where} \quad &\Gamma(Y) \equiv \left[\phi(Z = +0) - \phi(Z = -0)\right]_{X=X_{te}} \\ &\phi_Z(Z = +0) = \phi_Z(Z = -0) \end{aligned}\right\} \qquad (35)$$

Numerical method of solution

Outline of procedure. The method of solution is very similar to that generally adopted for two-dimensional problems. A uniform three-dimensional mesh is placed in the computing space, $|x| \leqslant 1$, $Y \leqslant 1$, $|Z| \leqslant 1$. The problem of solving the differential equation (29) is changed into one of solving a set of simultaneous algebraic equations, the unknowns being the values of ϕ at the mesh points or nodes, by replacing the derivatives with finite-difference approximations. Details of the approximations and the resulting algebraic equations are given below. The equations are solved by an adaptation of the iterative successive line relaxation technique used in two-dimensional calculations. To start the computation an initial estimate for ϕ throughout the field is needed. We assume for this that $\phi = 0$ everywhere, unless there is a suitable solution already available. The basic element in the computation is the simultaneous solution of the subset of algebraic equations for new values of ϕ on a vertical column $X = \text{const.}$, $Y = \text{const.}$, using values from the previous cycle of the iteration where necessary. The coefficients in the subset form a tridiagonal matrix and the equations are readily solved by triangular resolution of the matrix and back-substitution. The newly calculated values of ϕ are over- or under-relaxed with reference to the previous values, by factors determined by trial, and the computation then proceeds to the next column. A single cycle consists of a sweep through the whole field, re-evaluating ϕ on one line after another. The cycles are repeated until the changes in ϕ from one cycle to the next are less than some assigned small quantity, when the solution is considered to have converged.

Difference approximations. Mesh points are identified in the manner shown in Fig.3. At a typical mesh point (i,j,k) that is in the interior of the field away from boundaries, finite-difference approximations of different types are made according to whether the flow is subsonic ($\underline{A}^* > 0$) or supersonic ($\underline{A}^* < 0$), and subject to the rules for split derivatives given earlier. Where central-difference approximations are required we take

$$\left.\begin{aligned} \phi_X(i,j,k) &= \left(\phi_{i+1,j,k} - \phi_{i-1,j,k}\right)/(2\Delta X) \\ \phi_{XX}(i,j,k) &= \left(\phi_{i+1,j,k} - 2\phi_{i,j,k} + \phi_{i-1,j,k}\right)/(\Delta X)^2 \\ \phi_{XY}(i,j,k) &= \left(\phi_{i+1,j+1,k} - \phi_{i-1,j+1,k} - \phi_{i+1,j-1,k} + \phi_{i-1,j-1,k}\right)/(4\Delta X\Delta Y) \end{aligned}\right\} \qquad \ldots (36)$$

and similar expressions for ϕ_Y, ϕ_Z, ϕ_{YY}, ϕ_{ZZ} and ϕ_{XZ}.

Where backward-difference approximations are required we take

$$\left.\begin{aligned} \phi_X(i,j,k) &= \left(\phi_{i,j,k} - \phi_{i-2,j,k}\right)/(2\Delta X) \\ \phi_{XX}(i,j,k) &= \left(\phi_{i,j,k} - 2\phi_{i-1,j,k} + \phi_{i-2,j,k}\right)/(\Delta X)^2 \end{aligned}\right\} \qquad (37)$$

Note that the approximations for second derivatives recommended by Jameson[4] for numerical stability differ slightly from, and are slightly more complicated than these. We have tried Jameson's recommendations and have not so far found any improvement in stability or rate of convergence.

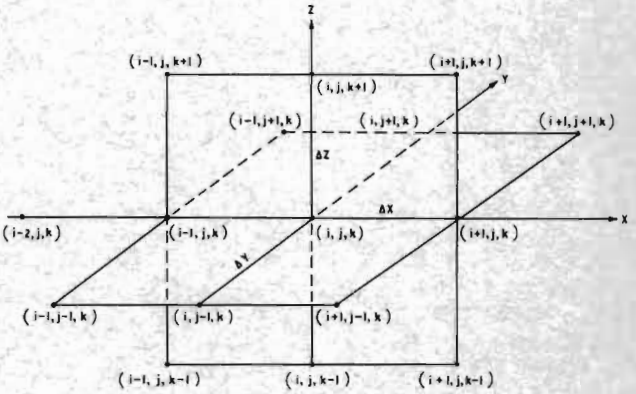

Fig.3 Mesh points in computing space

If we denote the value of ϕ evaluated in the current cycle by $\phi^{(n)}$ and that in the previous cycle by $\phi^{(n-1)}$, the precise form of the difference equation obtained by substituting the above difference approximations into equation (29) will depend on the ordering of the sweep through the field in each cycle. We sweep through successive planes $X = \text{const.}$ in the order of increasing X and in each plane we solve for ϕ on successive columns $Y = \text{const.}$ in the order of increasing Y. When the flow is subsonic ($\underline{A}^* > 0$) at the point (i,j,k) equation (29) becomes

$$d_k\phi^{(n)}_{i,j,k-1} + c_k\phi^{(n)}_{i,j,k} + b_k\phi^{(n)}_{i,j,k+1} = a_k \qquad (38)$$

where $d_k = C(\Delta X/\Delta Z)^2$

$$c_k = -2\left[\underline{A}^* + A + B(\Delta X/\Delta Y)^2 + C(\Delta X/\Delta Z)^2\right]$$

$$b_k = C(\Delta X/\Delta Z)^2$$

and

$$a_k = -\underline{A}^*\left(\phi^{(n-1)}_{i+1,j,k} + \phi^{(n)}_{i-1,j,k}\right) + f_k$$

where $f_k = -A\left(\phi^{(n-1)}_{i+1,j,k} + \phi^{(n)}_{i-1,j,k}\right)$

$- B(\Delta X/\Delta Y)^2\left(\phi^{(n-1)}_{i,j+1,k} + \phi^{(n)}_{i,j-1,k}\right)$

$- \tfrac{1}{2}D(\Delta X/\Delta Y)\left(\phi^{(n-1)}_{i+1,j+1,k} + \phi^{(n)}_{i-1,j-1,k} - \phi^{(n)}_{i-1,j+1,k} - \phi^{(n-1)}_{i+1,j-1,k}\right)$

$- \tfrac{1}{2}E(\Delta X/\Delta Z)\left(\phi^{(n-1)}_{i+1,j,k+1} + \phi^{(n)}_{i-1,j,k-1} - \phi^{(n)}_{i-1,j,k+1} - \phi^{(n-1)}_{i+1,j,k-1}\right)$

$- (\underline{G}^* + G)(\Delta X)^2$.

When the flow is supersonic ($\underline{A}^* < 0$) equation (29) becomes

$$d'_k\phi^{(n)}_{i,j,k-1} + c'_k\phi^{(n)}_{i,j,k} + b'_k\phi^{(n)}_{i,j,k+1} = a'_k \qquad (39)$$

where $d'_k = C(\Delta X/\Delta Z)^2$

$c'_k = -2\left[A - \tfrac{1}{2}\underline{A}^* + B(\Delta X/\Delta Y)^2 + C(\Delta X/\Delta Z)^2\right]$

$b'_k = C(\Delta X/\Delta Z)^2$

$a'_k = \underline{A}^*\left(2\phi^{(n)}_{i-1,j,k} - \phi^{(n)}_{i-2,j,k}\right) + f_k$.

Special difference approximations. Modifications of the above are needed where the symmetry, flow tangency and vortex sheet conditions are to be satisfied. When a point (i,j,k) lies on the plane of symmetry $Y = 0$ the symmetry conditions (34) are satisfied by putting

$$\left.\begin{aligned} \phi_{i-1,j-1,k} &= \phi_{i-1,j+1,k} \\ \phi_{i,j-1,k} &= \phi_{i,j+1,k} \\ \phi_{i+1,j-1,k} &= \phi_{i,j+1,k} \end{aligned}\right\} \qquad (40)$$

whenever these occur in equations (38) or (39).

The flow-tangency condition (20) is satisfied on $Z = \pm 0$ for each point (i,j,k) on the wing planform in the course of satisfying the governing differential equation (29) there. Accordingly the terms ϕ_Z, ϕ_{XZ} and ϕ_{ZZ} in equation (29) are not given by finite-difference approximations as indicated in equations (36). Instead, ϕ_Z is given by equation (30) and we set

$$\left.\begin{aligned} \left[\phi_{XZ}(Z = \pm 0)\right]_{i,j,k} &= \frac{1}{2\Delta X}\left\{\left[\phi_Z(Z = \pm 0)\right]_{i+1,j,k} - \left[\phi_Z(Z = \pm 0)\right]_{i-1,j,k}\right\} \\ \left[\phi_{ZZ}(Z = \pm 0)\right]_{i,j,k} &= \frac{2}{(\Delta Z)^2}\left\{\phi_{i,j,k\pm 1} - \phi_{i,j,k} \mp \Delta Z\left[\phi_Z(Z = \pm 0)\right]_{i,j,k}\right\} \end{aligned}\right\} \quad \ldots (41)$$

Note that the last is a one-sided, first-order approximation. Substitution of these into equation (29) yields, for subsonic and supersonic flows, difference equations which correspond to equations (38) and (39) respectively.

The vortex sheet conditions (25) are incorporated into a special difference equation, corresponding to equation (38) or (39), for points at $Z = +0$ on the sheet, and the condition

$$\left[\phi(Z = +0) - \phi(Z = -0)\right]_{X>X_{te}} = \Gamma(Y)$$

is used to evaluate $\phi(Z = -0)$. Care is needed because, although ϕ_X, ϕ_{XX} and ϕ_Z are continuous through the sheet, ϕ_Y, ϕ_{XY}, ϕ_{YY} and ϕ_{ZZ} are not. We first write down the two difference equations for the points at $Z = +0$ and $Z = -0$ respectively on either side of the sheet, using one-sided differences in the same way as when the points lie on the planform of the wing, but making use of the conditions that ϕ_X and ϕ_{XX} are continuous through the sheet. These equations necessarily include the unknown quantities $\phi_Z(Z = +0)$ and $\phi_Z(Z = -0)$ respectively, and both include $\phi(Z = +0)$ and $\phi(Z = -0)$. However, the conditions (25) enable us to eliminate all of these except $\phi(Z = +0)$ to obtain a single equation of the form (38) or (39), but with special expressions for the coefficients a_k, b_k, ...

Sample calculations

The above numerical method has been used for several calculations, for a variety of configurations and for free-stream Mach numbers ranging from 0.6 to 1.2. Although development and refinement of the method continues, an encouraging degree of reliability and versatility has been achieved. To illustrate this a selection of the calculated results is presented here. Except where otherwise stated we have taken $p = 1.95$, $q = 1$ and $r = 0$ in equation (29). The choice of 1.95 rather than 2.0 for p gives a slight but barely significant improvement in the agreement with the exact solutions shown in Fig.4. The choice $r = 0$ facilitates the treatment of wings with blunt leading edges where the perturbations are large. Instead of the expression for the pressure coefficient given by equation (12) we use the modification

$$C_p = -2\phi_x - \left(1 - M_\infty^2\right)\phi_x^2 - \phi_y^2 \qquad (42)$$

We begin a calculation with a coarse mesh, unless we are seeking only a small perturbation from a known solution, and complete the calculation with a $60 \times 25 \times 40$ mesh. A typical calculation of the flow about a given wing, for one free-stream Mach number M_∞ and one incidence α , and involving about 150 sweeps through the $60 \times 25 \times 40$ mesh, takes about 30 minutes to complete on an IBM 370/165 computer.

Fig.4 shows comparisons of calculated pressure distributions with solutions of the exact equation for the velocity potential by the method of Jameson[4], for a rectangular wing of aspect ratio 6 and having a NACA 0012 section. The exact solution differs considerably from that for the two-dimensional aerofoil, so this comparison does provide a test of reliability when the flow is three-dimensional as well as when the perturbations are not small and the free-stream Mach number is not near unity (in the sense that we do not have $1 - M_\infty^2 \ll 1$).

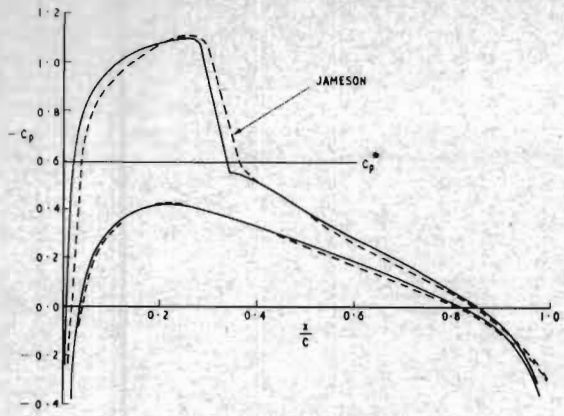

(a) Centre-section, $\eta = 0$

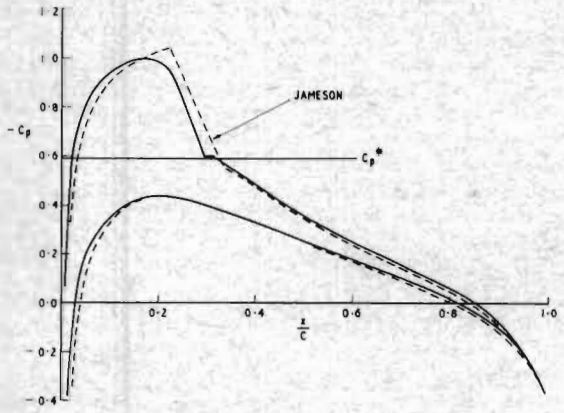

(b) 2/3 semi-span, $\eta = 0.667$

Fig.4 Comparison with solution of exact potential equation by method of Jameson[4] Rectangular wing, aspect ratio 6, NACA 0012 section. $M_\infty = 0.75$, $\alpha = 2^o$

For swept wings of symmetrical planform there are no such exact solutions available for comparison and so we make comparisons with experimental measurements in cases for which we expect viscous effects and wind-tunnel interference to be small. Comparisons are shown in Fig.5 with measurements made at RAE of the pressure distribution over the RAE Wing A at zero incidence. The wing planform is shown inset. The wing has a symmetrical RAE 101 section of 9% thickness and is not twisted. The comparisons show that fairly satisfactory results can be obtained for a wing of moderate sweep, at least for a simple non-lifting shape.

For lifting swept wings it is very difficult to draw useful conclusions from comparisons with experimental measurements, mainly because of the uncertainties in accounting for viscous effects. However, we have in such cases made comparisons with results obtained by Lomax, Bailey and Ballhaus.[10] Fig.6 shows calculated pressure distributions for a simulated C141 wing. Also shown is the effect of setting $q = 0$, which reduces our governing differential equation to essentially the same as that of Lomax *et al*. The change in pressure distribution, in switching from

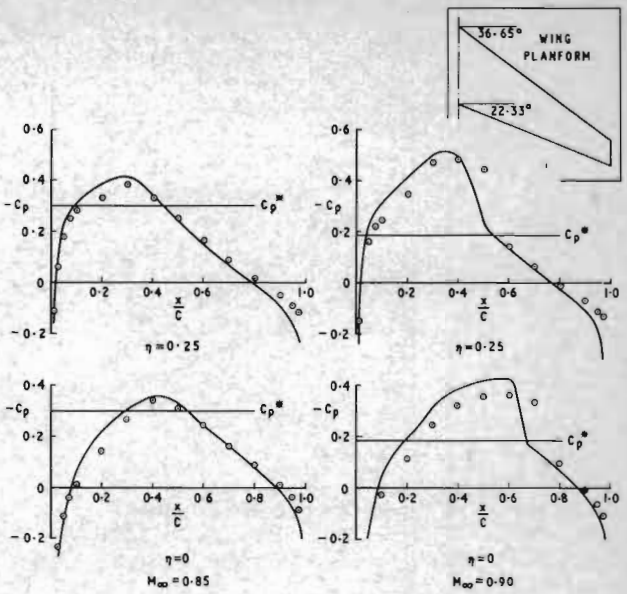

Fig.5 Comparison with measured pressures on RAE wing A. $\alpha = 0$, $R_e = 1.0 \times 10^6$

$q = 1$ to $q = 0$, is not negligible. The differences between the Lomax pressure distribution and that for $q = 0$ seem attributable to the differences in detail in the two methods of solution and, indeed, there is better agreement with more recent calculations by NASA.

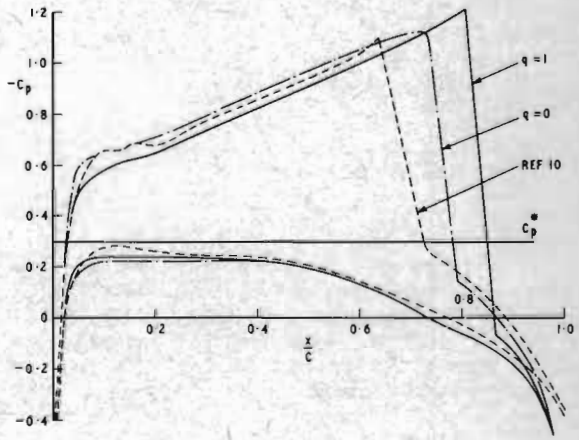

Fig.6 Calculated pressures on simulated C141 wing $M_\infty = 0.853$, $\alpha = 0$. Spanwise station $\eta = 0.693$

Figs.7 and 8 have been included to illustrate the versatility of the method. Fig.7 shows a calculated isobar pattern on the upper surface of a swept wing that is typical of modern transport design, with considerable twist and camber. Fig.8 shows the substantial difference in lift from that given by lifting-surface theory[11] when the flow is supercritical.

Remarks on further work

The work has now reached a stage where inviscid transonic flow about symmetrical wings

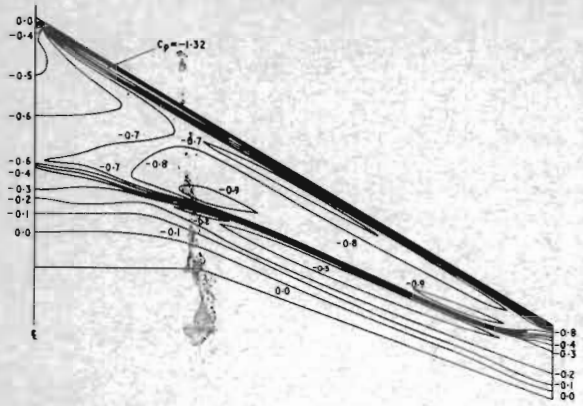

Fig.7 Calculated isobars on upper surface of RAE wing 759. $M_\infty = 0.84$, α (at crank) = 1.27°. $C_p^* = -0.32$, C_p^* (normal to leading edge) = -0.67

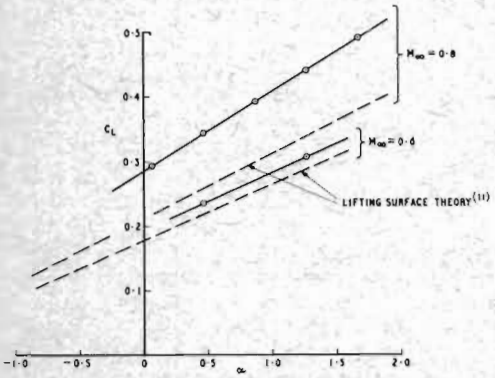

Fig.8 Calculated variations of lift coefficient with incidence. RAE wing 759

with arbitrary planform and arbitrary spanwise variation of section and twist can be calculated. Also, the calculations have appeared to be sufficiently accurate and economical for practical designers to use the method. So far little has been done to improve accuracy by refinements in the coordinate stretchings, or by empirical modifications of the governing equation or of the expression for the pressure coefficient, such as were found in two-dimensional calculations to be highly effective (and necessary) when perturbations were not small. Improvements in accuracy from modifications of these types should therefore be expected. One prerequisite here is the development of a method to take account of viscous effects, so that comparisons with experimental measurements can carry conviction.

Of course, much more than improvement in accuracy is needed, if designers are to be provided with all the computational tools they need. Obvious extensions of the present work for the immediate future are the inclusion of viscous boundary layers and wakes, as already mentioned above, an improved treatment of shock waves, for better predictions of shock pressure-rise, the development of methods for wing-body configurations, and the development of inverse design methods.

Some progress in these has already been made. The calculation of viscous effects for aerofoils is described in the second part of this paper. At ARA, Bedford, Langley and Forsey have already developed a design method to a stage at which successful designs for uncomplicated flows with single shocks have been obtained. The method is based on a modification of the direct method described here in which the surface flow-tangency boundary condition is replaced, over part of the wing, by a surface pressure boundary condition. The wing planform is fixed but otherwise there are a number of options in what is prescribed and what is to be calculated. An example is shown in Figs.9, 10 and 11, in which the leading-edge geometry, the overall thickness distribution and the upper surface pressure distribution aft of 10% chord are prescribed. Fig.9 shows the corresponding isobar pattern. The calculation begins with an initial solution obtained with the direct method for some wing with a guessed spanwise variation of camber and twist and yields, by an analogous iterative process of line relaxation, the spanwise variation of twist shown in Fig.10. Fig.11 shows calculated camber lines and the corresponding pressure distributions. Checks by forward direct calculation have shown that within the bounds of the theory such designs do indeed provide the required pressure distributions, with the shock essentially in the position and of the strength required.

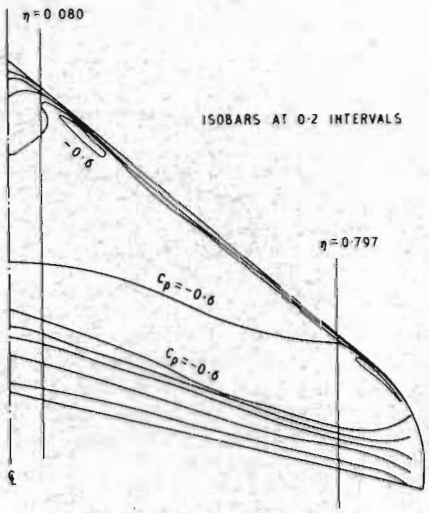

Fig.9 Isobars for specified upper surface pressure distribution on ARA wing

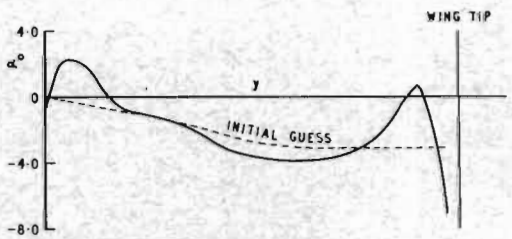

Fig.10 Calculated spanwise variation of twist of ARA wing

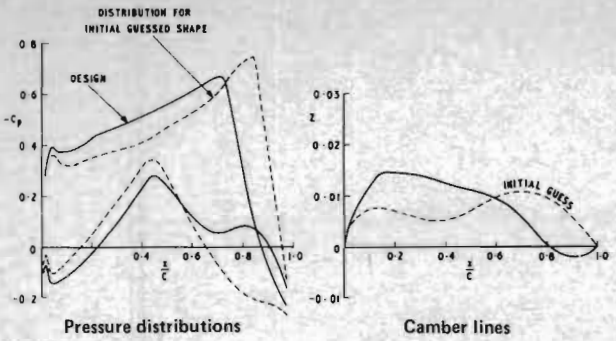

Pressure distributions Camber lines

(a) Spanwise station $\eta = 0.080$

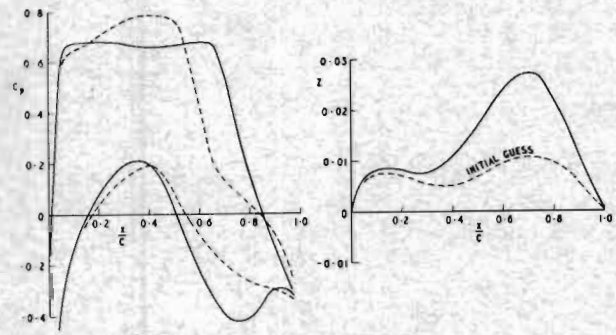

(b) Spanwise station $\eta = 0.797$

Fig.11 Pressure distributions and corresponding calculated camber lines for ARA wing

III. Estimation of viscous effects

General approach

In the first part of the paper we have considered an approximate method for the determination of the inviscid flow over a swept wing, but in practice the aircraft designer requires a design procedure which is applicable to compressible viscous flow and this remains the ultimate aim. In this part of the paper we consider the role played by viscosity in determining the characteristics of two-dimensional aerofoils as a first step in this direction. For many years the importance of viscous effects has been appreciated, but it has not been until comparatively recently, largely through the introduction of high speed digital computers into common usage, that it has been practicable to make much progress towards a calculation of the characteristics of an aerofoil in a real fluid, that is, a calculation with a reasonably realistic allowance for the existence of a boundary layer and a viscous wake.

Preston[12] showed how the rigid boundary of an aerofoil might be replaced by another equivalent boundary for the calculation of the representative inviscid flow exterior to the viscous layers. The equivalent boundary, or displacement surface as shown in Fig.12 is defined so that the streamlines of the inviscid flow over this surface enter the boundary layer or wake at approximately the correct angle and consequently the streamlines outside the viscous layers are correctly simulated. Such an equivalent boundary is formed by displacing the rigid boundary normal to itself by a small distance to account for the mass flux decrement in the viscous layers and by representing the wake by a similarly derived layer of finite thickness, whose position is determined by a relationship between the pressure difference across it, its thickness and its curvature. The pressures can therefore be obtained for the essentially inviscid flow over this boundary but with a prescribed pressure difference across the wake. A correction should then be applied to these pressures to derive the required prediction of the pressure coefficient on the actual wing surface.

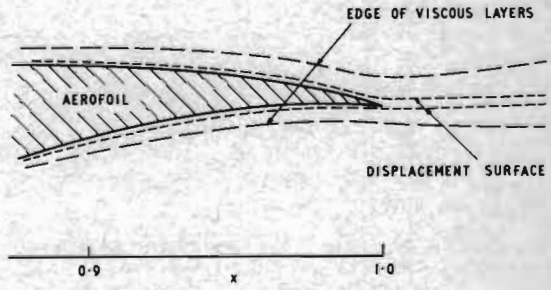

Fig.12 Typical viscous layers (Reynolds number = 10^7)

We have pre-supposed that a method exists for determining the displacement thickness of the boundary layer and wake. Near the trailing edge the boundary layer and wake grow in a pressure field with significant pressure gradients both along and normal to the local stream direction and, strictly, a theory is required for this class of flow, but in order to make further progress we assume that the growth is everywhere unaffected by normal pressure gradients and that the well established methods for the growth of the viscous layers may be used. The important integral parameters are, as we shall see later, the displacement and momentum thicknesses, and these may be obtained for a turbulent boundary layer and wake by any one of the well established methods. In the work we describe[13,14,15] we have chosen to consider only methods which are readily available, give sufficient accuracy, are applicable to the normal Reynolds number range for wind tunnel tests on aerofoils and which may be used for extrapolation to flight conditions. We found that aft of the location of boundary-layer transition and for attached flow the integral parameters required may be adequately obtained by the entrainment method of Green[16] for the pressure distributions encountered on single aerofoils at near cruise conditions in wholly subcritical flow, an example of which is given in Fig.13; but for cases with supercritical flow where shock waves are likely it is preferable to use the more recent 'lag' entrainment method.[17] Ahead of the transition the laminar layers have been determined by a version of Thwaites' approximate method[18] which is extended for compressible flow by the Stewartson-Illingworth transformation.[19] Since the subsequent development of a turbulent boundary layer when calculated by the entrainment methods is insensitive to the starting value for the shape factor ($H = \delta^*/\theta$) at transition, it has been assumed that the laminar value may be used; thus to some extent we get a boundary-layer development resembling a

rapid change from a laminar to a truly turbulent layer. It has also been assumed that the momentum thickness is continuous at transition except when it is necessary to increase its value to account for the influence of a transition trip.

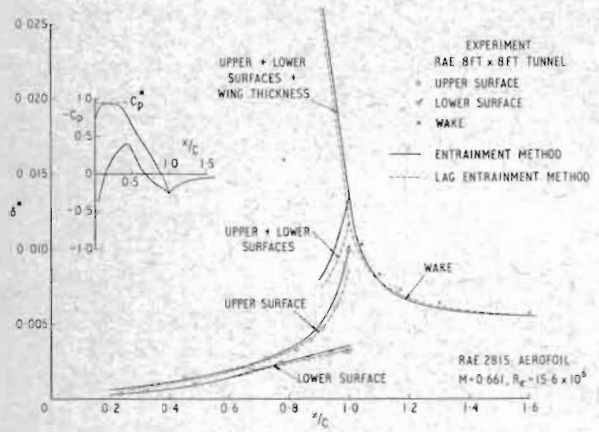

Fig.13 Viscous layer — displacement thicknesses

To determine the influence of viscous layers on the pressure distribution over an aerofoil we use an iterative scheme, since the growth of the boundary layer and wake depend on the overall pressure distribution and, in turn, the pressure distribution is modified as a result of the change in the growth of the viscous layers. It is fortunate that the changes in boundary conditions due to viscous effects, other than those close to the trailing edge of the aerofoil and in the region of a shock, are not excessive and consequently it has been found possible to set up suitable iterative procedures, similar in essence to the procedure used by Lock, Wilby and Powell.[20]

Modified boundary conditions

The modification of any inviscid flow method to include an allowance for viscous effects as originally suggested by Preston requires the modification of the boundary conditions while retaining the same governing differential equations, and in principle it allows the vast experience of inviscid flow methods to be utilized. Also, since the displacement surface is usually much thinner than the aerofoil thickness, it is possible to allow for the effect of the displacement surface by altering the boundary conditions at the original surface or at the original place of application instead of at the displacement surface.

Let us now consider the elements of flow shown in Fig.14. We need to represent the models of the viscous flow (Figs.14a and 14b), by a corresponding inviscid model (Fig.14c). It is possible to show[13] that the difference in pressure across a viscous layer that has a velocity defect is less than that across a corresponding inviscid layer of the same thickness and curvature but without a velocity defect by an amount that is approximately given by

$$\left(\frac{\Delta P}{\tfrac{1}{2}\rho_\infty U_\infty^2}\right)_{\text{inviscid}} - \left(\frac{\Delta P}{\tfrac{1}{2}\rho_\infty U_\infty^2}\right)_{\text{viscous}} = -2\frac{d^2Z}{dx^2}(\delta^* + \theta). \quad \ldots (43)$$

For a boundary layer or wake, considering only the part above the dividing streamline, we have from equation (43) using the definitions given in Fig.14:

$$\frac{P_{\delta,u} - P_{u,i}}{\tfrac{1}{2}\rho_\infty U_\infty^2} - \frac{P_{\delta,u} - P_u}{\tfrac{1}{2}\rho_\infty U_\infty^2} = -2\frac{d^2Z_u}{dx^2}(\delta_u^* + \theta_u) \quad (44)$$

and for the lower side of the wake or the boundary layer below the wing we have

$$\frac{P_{\delta,\ell} - P_{\ell,i}}{\tfrac{1}{2}\rho_\infty U_\infty^2} - \frac{P_{\delta,\ell} - P_\ell}{\tfrac{1}{2}\rho_\infty U_\infty^2} = +2\frac{d^2Z_\ell}{dx^2}(\delta_\ell^* + \theta_\ell) \quad (45)$$

whence

$$\frac{P_{u,i} - P_{\ell,i}}{\tfrac{1}{2}\rho_\infty U_\infty^2} - \frac{P_u - P_\ell}{\tfrac{1}{2}\rho_\infty U_\infty^2} = 2\left[\frac{d^2Z}{dx^2}(\delta^* + \theta)\right]_{\text{upper}} + 2\left[\frac{d^2Z}{dx^2}(\delta^* + \theta)\right]_{\text{lower}} \quad (46)$$

where $(P_u - P_\ell)/(\tfrac{1}{2}\rho_\infty U_\infty^2)$ is the pressure coefficient required across the wing, and $(P_{u,i} - P_{\ell,i})/(\tfrac{1}{2}\rho_\infty U_\infty^2)$ is the pressure coefficient applicable to the inviscid flow model. It should be noted that $P_u = P_\ell$ and $[d^2Z/dx^2]_{\text{upper}} = [d^2Z/dx^2]_{\text{lower}}$ for the wake. So using an inviscid flow model we may simulate approximately the conditions for the viscous flow by changing the wing boundary conditions, including an extension of the wing boundary into the wake. In a similar way we may consider the influence of the displacement effect of the layers as a change in the boundary conditions at the same wing boundary.

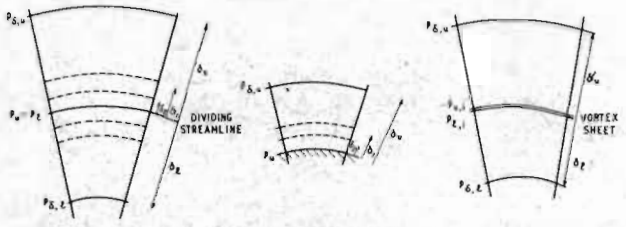

(a) Viscous model of wake (b) Viscous model of boundary layer (c) Inviscid model of wake

Fig.14 Elements of curved flow

The procedure outlined above indicates how the dominant terms from the influence of the viscous layers might be included; it cannot be claimed to be more than approximate and the result of any such procedure must be judged by comparison with experimental results.

The iterative schemes

The interaction between the inviscid flow and the viscous flow is obtained by integrating the methods available into a single program; the operating cycle commences with a given geometry, Mach number, incidence and Reynolds number with fixed transition points for each surface. The first part of the calculation involves calculating the inviscid pressure distribution for the actual aerofoil, but it may be necessary to start the calculation at a lower angle of incidence, say at an angle which gives approximately the required C_L, in order to

avoid extreme conditions which will not be encountered later in the calculation. If in practice the inviscid flow method itself involves an iterative procedure, such as described in the first part of the paper, then it is unnecessary to obtain a fully converged solution before calculating the boundary layer and wake development.[14] Instead the 'inviscid' cycle proceeds until the convergence parameter ε is less than some constant which is sufficiently low to ensure that the correct form of pressure distribution is obtained. At this stage the boundary layer and wake displacement thicknesses are calculated for this pressure distribution, but some adjustment of the growth of the viscous layers may be necessary in order to suppress the influence of the singular behaviour of the velocity at the trailing edge and so avoid, at this initial stage of the procedure, any separation of the boundary layer near that point.

The next stage is to revise the numerical values for the boundary conditions. The ordinates for the new displacement surface are obtained by adding a proportion of the displacement thickness of the boundary layer to the aerofoil ordinates as follows,

$$Z_{(1)u} = Z_u + k\delta^*_{(1)u} \quad , \tag{47}$$

and

$$Z_{(1)\ell} = Z_\ell - k\delta^*_{(1)\ell} \qquad \text{for} \quad 0 < x \leqslant 1 \tag{48}$$

where k is a numerical constant. The thickness of the wake is taken as

$$Z_{(1)t} = k\left(\delta^*_{(1)u} + \delta^*_{(1)\ell}\right) \quad , \text{ for } \quad x > 1 \tag{49}$$

while the pressure difference across the dividing streamline is taken as

$$\Delta C_p = 2k \frac{d^2Z}{dx^2}\left(\delta^*_{(1)u} + \delta^*_{(1)\ell} + \theta_{(1)u} + \theta_{(1)\ell}\right) \quad , \tag{50}$$

and d^2Z/dx^2 ($\doteq dw/dx$ on the dividing streamline or point at which boundary conditions are applied) is obtained from the current solution of the inviscid flow section of the program.

At this stage we return to the inviscid element of the program, with modified boundary conditions, interpolating the data if necessary. A typical scheme for the calculation is sketched in Fig.15.

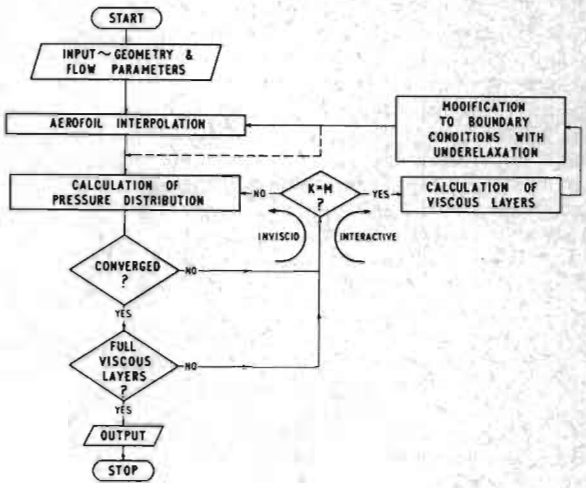

Fig.15 Interactive iterative scheme

For all iterations after the first, the boundary conditions are modified from the previous set using a relaxation procedure. So equations (47) to (50) become for subsequent iterations,

$$Z_{Nu} = (1 - k)Z_{(N-1)u} + k\left(Z_u + \delta^*_{(N)u}\right) \tag{51}$$

$$Z_{N\ell} = (1 - k)Z_{(N-1)\ell} + k\left(Z_\ell - \delta^*_{(N)\ell}\right) \tag{52}$$

$$Z_{Nt} = (1 - k)Z_{(N-1)t} + k\left(\delta^*_{(N)u} + \delta^*_{(N)\ell}\right) \tag{53}$$

$$\Delta C_{pN} = (1 - k)\Delta C_{p(N-1)} + k\left[2\frac{dw}{dx}\left(\delta^*_{(N)u} + \theta_{(N)u} + \delta^*_{(N)\ell} + \theta_{(N)\ell}\right)\right] \tag{54}$$

where N is the number of the iteration for the interactive path, and the factor k has been limited to 0.2 for a case where the boundary layer is well away from separation near the trailing edge. In addition to the above equations (51) to (54), the angle of incidence is increased at a rate related to k until the required angle is reached.

For calculations which include an 'iterative' cycle for the inviscid flow as indicated in Fig.15, it has been found convenient to interrupt this cycle every M iterations to update the boundary conditions. The value of M is chosen by experience so that the full viscous layers have been included before the convergence of the 'inviscid' cycle is indicated. The convergence of the 'interactive' cycle is then checked by continuing the program for one more interactive cycle with $k = 1$, so that the boundary conditions are obtained completely from the current viscous flow calculation, and then resuming the full scheme until convergence is again achieved for the 'inviscid' cycle. By using such a procedure it has been possible to reach converged solutions with only a 20-30% increase in computing time compared with a solution for inviscid flow at similar conditions. In addition an intermediate solution may be saved and used as a starting solution if further solutions for the same aerofoil are required at other initial conditions, of Mach number, Reynolds number, transition positions, or incidence.

Choice of inviscid flow method

The 'viscous' method described in the previous section assumed the existence of a suitably modified method for inviscid flow. Ideally this should be a method which can be extended to three-dimensional flows and sufficiently close to an 'exact' method that any uncertainties will be small compared with those due to the approximation made in inserting an allowance for the viscous layers. At this stage rapid advances are being made with finite-difference methods for the 'exact' potential equations; but the methods available when this work was commenced were based on the small-perturbation concept and these will be used in the work described here.

We will now consider two examples, for the 12% thick RAE 2822 aerofoil, to indicate the accuracy obtained for pressure distributions similar in form to those obtained in later examples for the viscous flow. Other examples are available, for instance in Refs.6 and 22. In Fig.16 a calculation by the nominally exact method of Sells[21] is compared with solutions from the 'subcritical' inviscid flow method used at RAE[22] (often called the first-order Standard Method), and from the 'supercritical' inviscid flow method, called Transonic Small-Perturbation Method (TSP), mentioned in the earlier part of the paper.[6] This example is an exacting test for both the approximate methods, since the 'subcritical' one is based on an incompressible flow concept with corrections for compressibility and the 'supercritical' one is based on the transonic small-perturbation concept which is 'tuned' to be used at higher speeds and not for a pressure distribution such as this where the flow is wholly subcritical. Both methods show an underestimation of the local suctions over the region of the 'roof top' in the pressure distribution on the upper surface but they both show good agreement with the exact solution over the rear of the aerofoil. This is a most important region to be considered when designing an aerofoil for attached 'viscous' flow. The other example (Fig.17) is for the same aerofoil at a higher Mach number. Here the 'exact' theory is obtained by the method of Garabedian and Korn[23] where the full equations are solved for steady potential flow by a finite difference method but no account is taken of the entropy changes across any shock waves which appear in the flow, and no attempt is made to ensure the conservation of mass or momentum across such a discontinuity. In this respect it is similar to the small-perturbation method and neither can be considered a truly exact solution. The example given is for an extreme case where the strength of the shock wave is higher than is likely to exist in viscous flow without separation of the boundary layer, even so the agreement is remarkably good, except that the shock wave is slightly stronger for the transonic small-perturbation method and differences exist in the pressure recovery behind the shock wave similar in form to those existing sometimes in comparisons between comparable 'exact' methods. Although the examples given are for one aerofoil the discrepancies are similar in magnitude to those found for a wider range of examples, and the small-perturbation methods are certainly acceptable as the basis of a viscous flow method which is required for engineering design purposes.

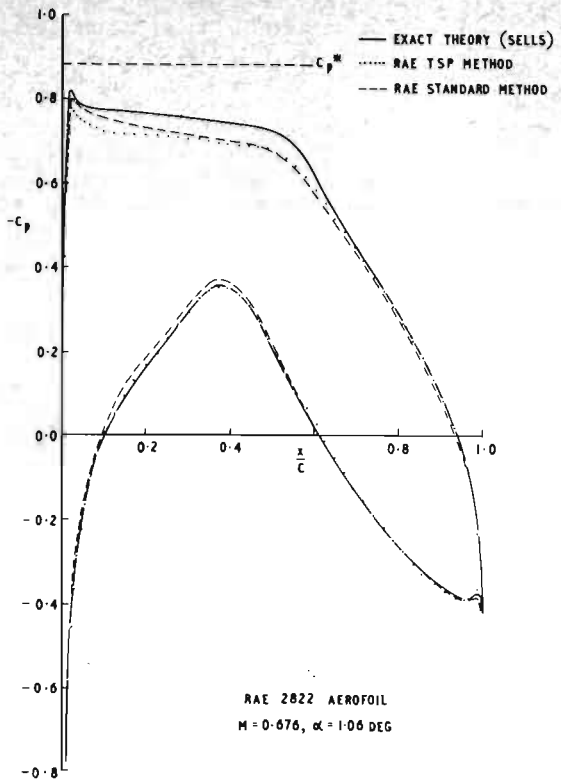

Fig.16 Comparison between various methods (inviscid subcritical flow)

Experimental evidence

Before making comparisons between the scheme proposed for viscous flow and experimental evidence it is worth considering the accuracy of information obtained in wind tunnels. Valid comparisons can be made only if the necessary corrections for tunnel constraints are adequate. It is well known that relatively large corrections are necessary when making measurements of the loads on two-dimensional aerofoils in wind tunnels[24] and there is a high degree of uncertainty about the magnitude of these corrections for tests in tunnels with slotted[25] or perforated walls. It is not uncommon for the measurements of lift-curve-slope, measured in different facilities at nominally the same conditions of Mach number, Reynolds number and transition positions to differ by 5% or more even for wholly subcritical flow. The reasons for these differences are difficult to establish but can be connected partly with the influence of end wall boundary-layer interference, the tests being done in rigs where the span of the aerofoil is insufficient to establish truly two-dimensional flow. At higher speeds where the flow is supercritical, with a shock wave established on the upper surface, some evidence exists from tests at comparatively low Reynolds numbers based on the chord (1×10^6) of disturbances from the end walls spreading across the span up to about 0.7 chords.[26] This suggests that significant end wall interference may exist in measurements made where the span/chord ratio of the panel is 1.4 or less and ideally this ratio should be much higher. Additionally Murman[27] has cast doubt on the conventional methods of correcting for wind tunnel wall interference where the conditions are such that a

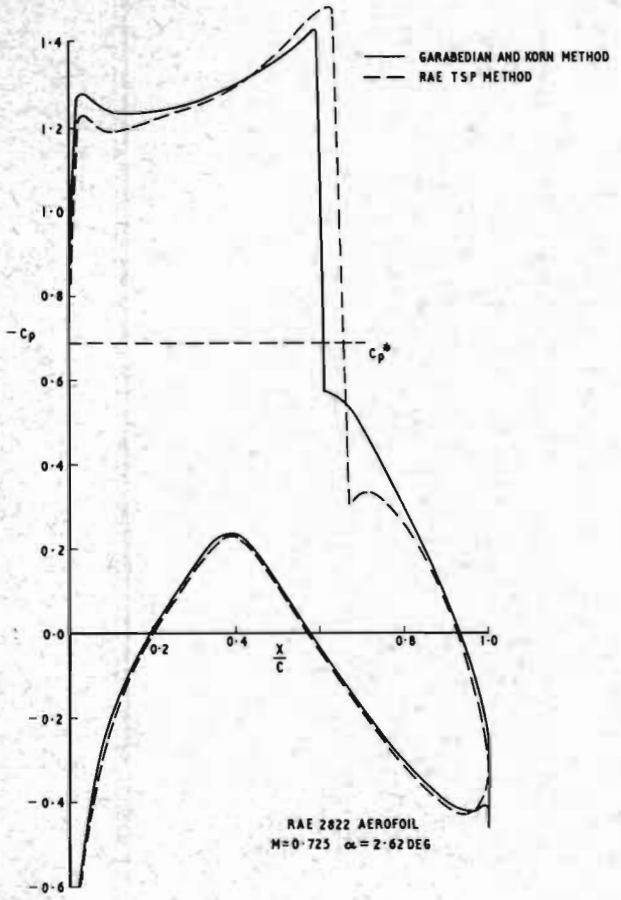

Fig.17 Comparison between methods (inviscid supercritical flow – strong shockwave)

significant region of supercritical flow exists between the aerofoil surface and the tunnel wall. Although the methods suggested in the present paper can be extended, as suggested by Murman, to include such tunnel wall constraints, the correction is yet another factor which causes uncertainty about the experimental evidence. As with the conventional method doubt exists about the magnitude of the parameters needed to specify the boundary conditions at the tunnel walls.

In this paper we will consider only recent experiments at RAE where interference effects have been reduced as far as possible, by keeping the model cross-sectional area small (0.3 × tunnel cross-sectional area or less), and the model aspect ratio and tunnel height/aerofoil chord ratio relatively high (3.0 and 4.0 respectively). Even in these experiments however, the situation regarding wind-tunnel corrections cannot be regarded as entirely satisfactory, particularly when extensive regions of supercritical flow are present.

Magnitude of effect

The methods outlined above give us an opportunity to assess the magnitude of the viscous effects for a range of examples where the flow may include supercritical regions and shock waves. In the first example (Fig.18) the 'subcritical-flow' method[13] is used for a flow that is wholly subcritical and in which the boundary layers are comparatively thin, even in the region of the trailing edge. It is notable that the magnitude of the effect of viscosity is estimated to be quite small for this example, and the change in lift is only of the same order as the uncertainty in experimental evidence mentioned previously. In the second example, which is for predominantly sub-critical flow (Fig.19) the effects of viscosity are much larger, because of increased rear loading and the consequential rapid thickening of the boundary layer over the rear part of the aerofoil. In this example the influence of the viscous layers account for a loss in lift of about 20% compared with the value for inviscid flow. For this example results

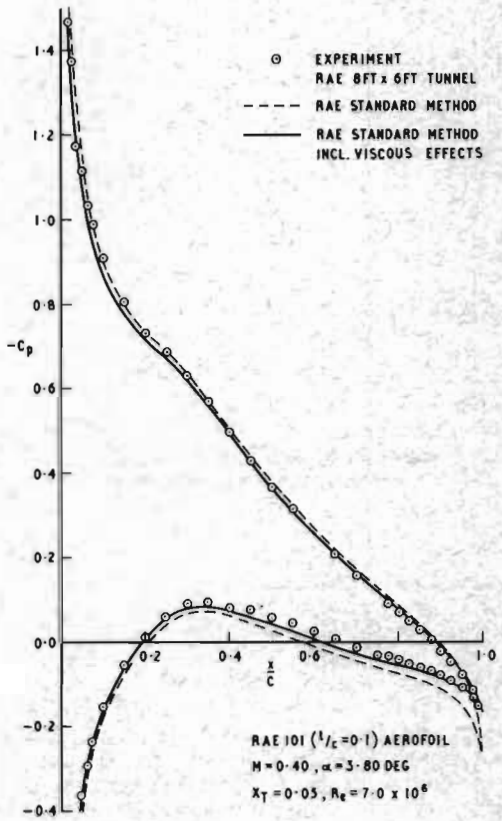

Fig.18 Conventional aerofoil (subcritical flow)

from both calculation methods are included, as well as the experimental results, which have been corrected by conventional means for tunnel effects. The deficiency in the methods ahead of mid-chord on the upper surface can be explained by the underestimation of velocities on the upper surface mentioned earlier for the 'inviscid' flow methods used (Fig.16) but the underestimation of the influence of the boundary layer ahead of about 40% chord on the lower surface is unexplained. In spite of these deficiencies the method appears to estimate the influence of viscosity encouragingly well.

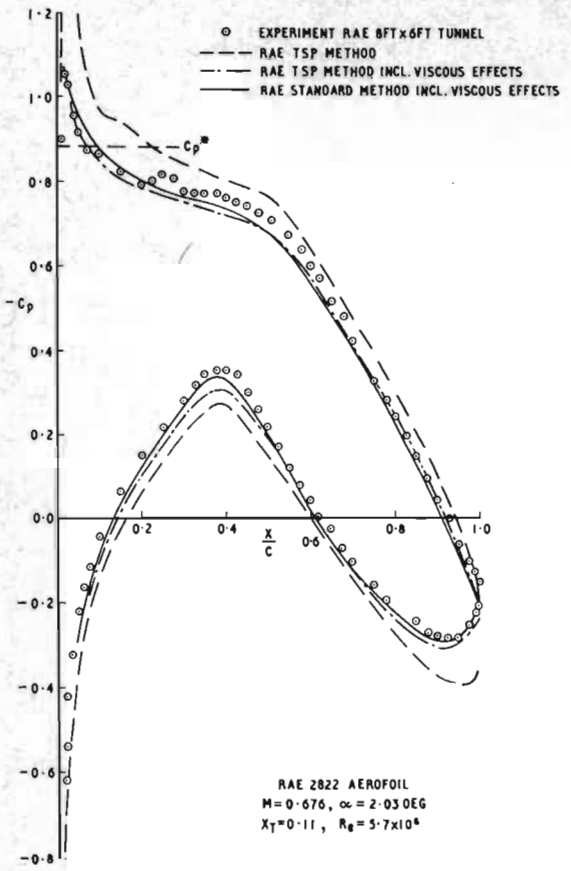

Fig.19 Rear loaded aerofoil (predominately subcritical flow)

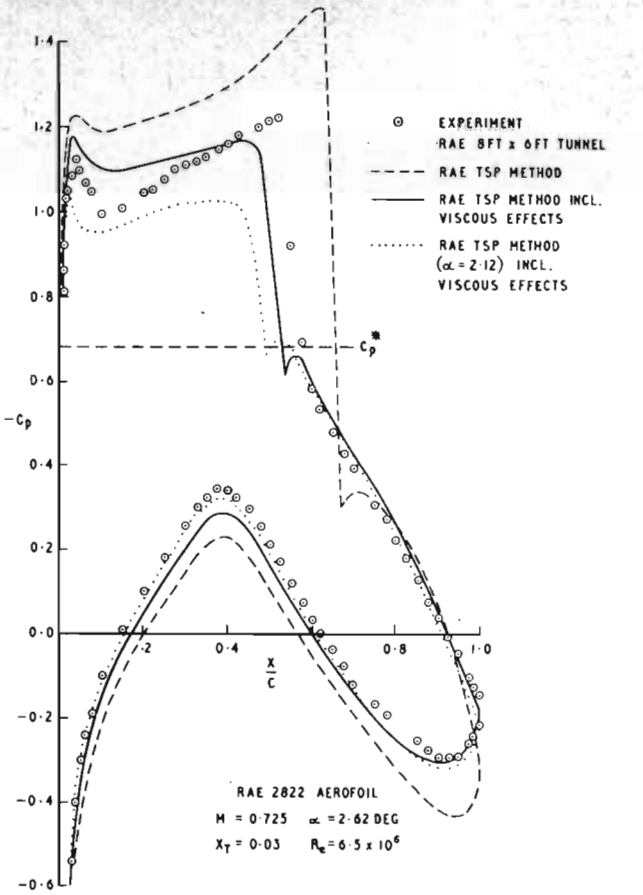

Fig.20 Rear loaded aerofoil (supercritical flow)

In the next example (Fig.20) larger differences exist, primarily because of the additional thickening of the boundary layer in the region of the shock wave. The lag entrainment method for determining the integral parameters of the boundary layer calculates values for the boundary-layer shape factor, in the region of the shock wave, which are rising rapidly towards a value normally associated with separation of the boundary layer. Under these circumstances it is by no means certain that the boundary-layer method can adequately represent the correct growth of the viscous layers locally. The difference between the inviscid flow and viscous flow methods under these conditions suggest a loss of lift due to viscous effects amounting to about 25% of the 'inviscid' value. The evidence from the experiments is not nearly so conclusive in this example, for although the pressure distribution over the rear of the aerofoil appears to be adequately predicted, it appears that the underestimation of the influence of the boundary layer ahead of about 40% chord on the lower surface still exists, and the shock wave is aft of the position predicted. It is not clear whether these discrepancies arise from the uncertainty about wind-tunnel corrections mentioned earlier or are due to an inadequacy in the method of treating the viscous effects. The comparisons suggest that better agreement might be achieved with a lower theoretical angle of incidence but this results in the shock wave being predicted further forward on the chord, as given by the dotted line for a case with the angle of incidence 0.5 degree lower than the actual value. These differences are unlikely to be explained by an inadequacy of the inviscid flow element used unless it is due to the failure to account correctly for the conservation of mass or momentum correctly across the discontinuity representing the shock wave. Some evidence exists[8] that the position of the shock waves can be significantly changed by attempting to improve the conditions across the shock wave.

The calculations at two incidences shown in Fig.20 make it clear that once aerofoils have significant rear loading it is insufficient to consider the influence of the boundary layer simply as a change in effective incidence.

An example of scale effects

No discussion of the influence of viscous effects on the pressure distribution over an aerofoil would be complete without some statement on the changes likely to occur when extrapolating measurements made in a wind tunnel to full-scale conditions. In Fig.21 measurements are given which show the difference in pressure distribution measured when an aerofoil is tested at the same incidence and Mach number, but at different chord Reynolds numbers with boundary-layer transition maintained close to the leading edge. At the lower Reynolds number there is some evidence of a gross disturbance in

the region of the transition fixing which may have thickened the boundary layer thus exaggerating the apparent scale effect to some extent. This disturbance was due to the relatively large transition fixing trip required at the low Reynolds number. Increasing the Reynolds number results in an increased pressure recovery near the trailing edge and some increase in rear loading. There is also a significant change in the development of the pressure distribution in the supercritical region consistent with an increase in effective incidence and with the shock wave correspondingly further aft. In Fig.22 predicted pressure distributions are given for conditions identical to those shown in the previous figure together with another case for a higher Reynolds number appropriate to full scale conditions. The trend of the results is very similar to that found experimentally, the graphs show the same general features discussed previously. It does appear however, that the changes with Reynolds number are not as large as found experimentally, but this is probably partly due to the thickening of the boundary layer at transition in the lower Reynolds number case. This point is illustrated further in Fig.23 where the normal force coefficient obtained by integrating the pressure distribution is plotted against Reynolds number based on the aerofoil chord. An allowance ($\Delta\theta u = 0.0002$) was made for the additional thickening of the boundary layer at transition and this is shown to account for some of the difference between the measurement and the theory at the lower Reynolds number.

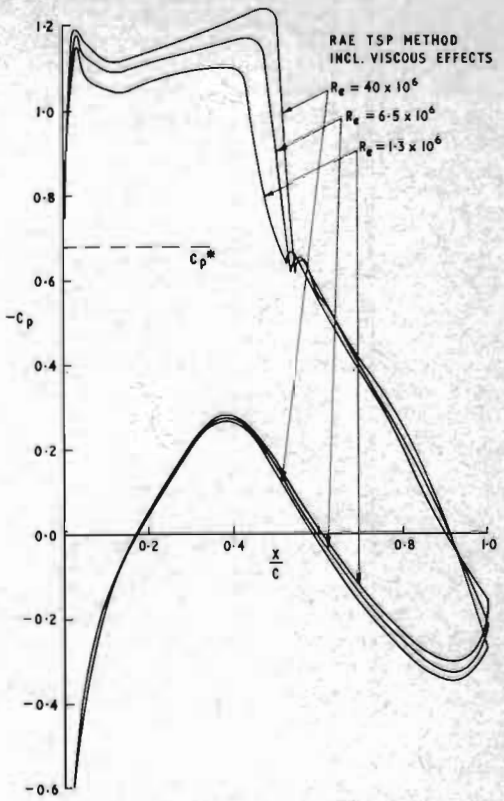

Fig.22 Scale effect on pressure coefficients (RAE 2822 aerofoil, M = 0.725, α = 2.62 deg, X_T = 0.03)

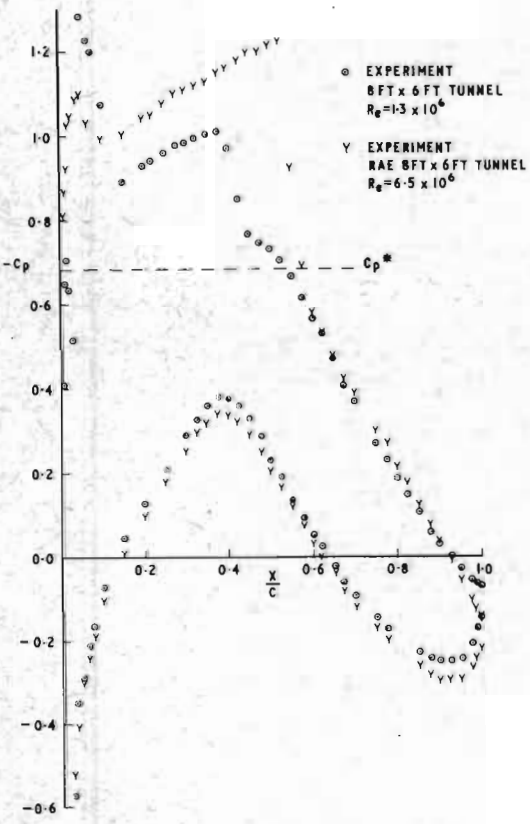

Fig.21 Scale effect on pressure coefficients (RAE 2822 aerofoil, M = 0.725, α = 2.62 deg, X_T = 0.03)

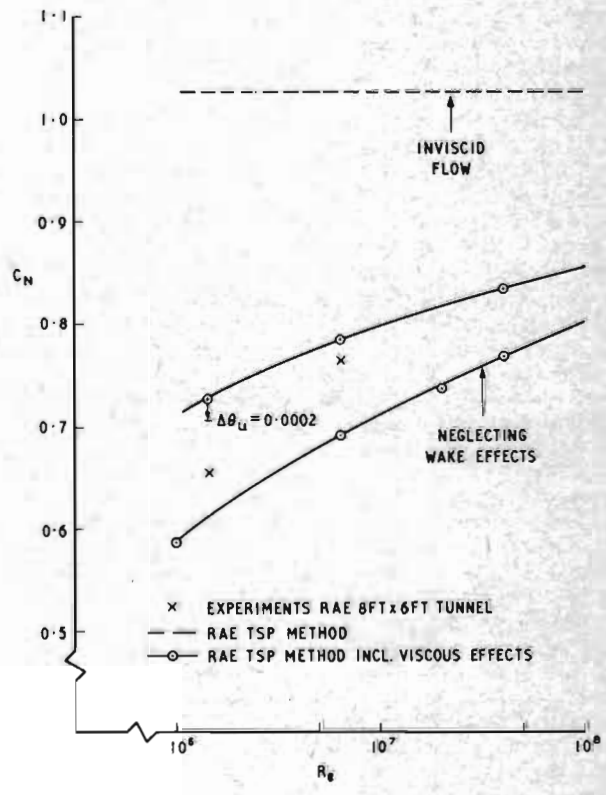

Fig.23 Scale effect on lift (RAE 2822 aerofoil, M = 0.725, α = 2.62 deg, X_T = 0.03)

In making estimates of the influence of viscous effects for engineering purposes it is tempting to ignore the influence of the wake and the corresponding curvature effects, thus including only the changes due to the displacement effect over the aerofoil. Although this goes some way to making an allowance for viscous effects there are significant differences due to the displacement and curvature effects of the wake as illustrated in Fig.23.

Concluding remarks

Although this section of the paper has been restricted to attached flow, the influence of the viscous layers has been shown to make a significant difference to the pressure distribution and loads on aerofoils. It suggests than an allowance for the viscous layers should be included in any method which will be used for the design of wings, and that for attached flow a reasonably realistic estimate may be made using the concept of a displacement surface with special boundary conditions in the wake. It appears that it is not sufficient to consider the influence of the boundary layer as an effective change in incidence alone as had been the practice for conventional aerofoils without significant near loading.

References

1 Edwards, J.B., "Future swept-wing transport aircraft options with reference to fuel price and the conservation of fuel," unpublished RAE note, 1974.

2 Murman, E.M., and Cole, J.D., "Calculation of plane steady transonic flows," *AIAA Journal*, Vol.9, No.1, pp.114-121 (1971)

3 Albone, C.M., "A finite difference scheme for computing supercritical flows in arbitrary coordinate systems," RAE Technical Report in preparation.

4 Jameson, A., "Iterative solution of transonic flows over airfoils and wings, including flows at Mach 1," to appear in *Comm. Pure Appl. Math.*

5 Albone, C.M., Hall, M.G., and Joyce, Gaynor, "A method for computing transonic flow about thin lifting wings," RAE Technical Report in preparation.

6 Albone, C.M., Catherall, D., Hall, M.G., and Joyce, Gaynor, "An improved numerical method for solving the transonic small-perturbation equation for the flow past a lifting aerofoil," RAE Technical Report 74056 (1974).

7 Ballhaus, W.F., and Bailey, F.R., "Numerical calculation of transonic flow about swept wings," AIAA Paper 72-677, June 1972.

8 Bailey, F.R., "On the computation of two- and three-dimensional transonic flows by relaxation methods," *Progress in Numerical Fluid Dynamics*, AGARD Lecture Series No.63 (1974)

9 Cole, J.D., "Twenty years of transonic flow," Boeing Scientific Research Laboratories Document DI-82-0878, July 1969.

10 Lomax, H., Bailey, F.R., and Ballhaus, W.F., "On the numerical simulation of three-dimensional transonic flow with application to the C-141," NASA TN D-6933 (1973).

11 Lehrian, Doris E., and Garner, H.C., "Theoretical calculation of generalized forces and load distribution on wings oscillating at general frequency in a subsonic stream," ARC R & M 3710, July 1971.

12 Preston, J.H., "The calculation of lift taking account of the boundary layer," ARC R & M 2725 (1949).

13 Firmin, M.C.P., "The calculation of pressure distribution, lift and drag, on single aerofoils at subcritical speeds. Part 1 Interim Method," RAE Technical Report 72235 (1973).

14 Jones, A.F., and Firmin, M.C.P., "On the calculation of viscous effects on the supercritical flow over an aerofoil," RAE unpublished 1973.

15 Firmin, M.C.P., and Jones, A.F., "The calculation of pressure distribution, lift and drag, on single aerofoils at supercritical speeds," RAE Technical Report in preparation (1974).

16 Green, J.E., "Application of Head's entrainment method to the prediction of turbulent boundary layers and wakes in compressible flow," RAE Technical Report 72079 (1972).

17 Green, J.E., Weeks, D.J., and Brooman, J.W.F., "Prediction of turbulent boundary layers and wakes in compressible flow by a lag-entrainment method," RAE Technical Report 72231 (1973).

18 Rosenhead, L., (Editor), "Laminar Boundary Layers, Fluid Motion Memoirs," Oxford University Press (1963).

19 Curle, N., "The Laminar Boundary-Layer Equations," Oxford Mathematical Monographs (1962).

20 Lock, R.C., Wilby, P.G., and Powell, P.J., "The prediction of aerofoil pressure distribution for sub-critical viscous flows," *The Aeronautical Quarterly*, Vol.XXI, Part 3 (1970).

21 Sells, C.C.L., "Plane subcritical flow past a lifting aerofoil," Proc. Roy. Soc. A 308, pp.377-401 (1968).

22 —— "A second-order method for estimating the sub-critical pressure distribution on a two-dimensional aerofoil in compressible inviscid flow," ESDU TD Memor. 72025 (to be issued).

23 Bauer, F., Garabedian, P.R., and Korn, D.G., "A Theory of Supercritical Wing Sections, with Computer Programs and Examples," Lecture Notes in Economics and Mathematical Systems, p.66, Springer-Verlag (1972).

24 Garner, H.C., Rogers, E.W.E., Acum, W.E.A., and Maskell, E.C., "Subsonic wind tunnel corrections," AGARDograph 109 (1966).

25 Firmin, M.C.P., and Cook, T.A., "Detailed exploration of the compressible, viscous flow over two-dimensional aerofoils at high Reynolds numbers," ICAS Conf. Paper 11/68 (1968).

26 Pierce, D., "The influence of end walls observed during tests of a two-dimensional aerofoil at M = 0.70," RAE (unpublished).

27 Murman, E.M., "Computation of wall effects in ventilated transonic wind tunnels," AIAA Paper 72-1007 (1972).

D I S C U S S I O N

R. Legendre (ONERA, Chatillon, France): I was much interested by the practical aspect of your results, Dr. Hall. We will have opportunities to discuss them at length.

For the moment, you will not be surprised if I ask what condition you apply to the edges of the wing. I understood you are interested by low practical incidence and do not take into account separation at the edges.

M.G. Hall and M.C.P. Firmin: The flow is assumed to be attached. We do not admit separation from the leading edges. Difficulties associated with the singularity at the leading edge in small-perturbation theory are avoided by ensuring that the mesh or grid

points of the numerical calculation do not lie in the leading edge.

H. Portnoy (Dept. of Aeronautical Engineering, Technion, I.I.T., Haifa, Israel): In the example of an inverse (design) problem given, the calculated twist diverged unrealistically towards the tip.

Did the author know of any restrictive criterion for inclusion in the wing planform-pressure-distribution specification to avoid this unrealistic shape resulting?

M.G. Hall and M.C.P. Firmin: The example was intended to illustrate the method rather than to show a realistic or practical twist distribution. If the pressure distribution that is specified leads to an unrealistic shape we conclude that a different pressure distribution is needed. There is no provision in the method for excluding pressure distributions that lead to unrealistic shapes.